

PREPARED FOR SUBMISSION TO JINST

XVTH WORKSHOP ON RESISTIVE PLATE CHAMBERS AND RELATED DETECTORS - RPC2020

10-14 FEBRUARY, 2020

ROME, ITALY

Numerical study of space charge electric field inside Resistive Plate Chamber

Tanay Dey,^{a,c,1} Supratik Mukhopadhyay,^{a,b} Subhasis Chattopadhyay,^c Jhiliam Sadukan^c

^a*Homi Bhabha National Institute,
Mumbai, India*

^b*Saha Institute of Nuclear Physics,
Kolkata, India*

^c*Variable Energy Cyclotron centre,
Kolkata, India*

E-mail: tanay.jop@gmail.com

ABSTRACT: Resistive plate chamber (RPC) is one of the state-of-the-art particle detection technology for the High Energy Physics (HEP) experiments. The basic operating mechanism of an RPC involves ionization of gas due to the passage of charged particles followed by electron transport, avalanche, and subsequent electromagnetic induction on readout strips due to the movement of the electrons and ions. Especially during streamer mode of operation, the electric field applied to the RPC can get significantly modified due to the presence of a large number of electrons and ions. In this study, we have worked on dominant issues related to the estimation of the electric field due to the space charge arising out of the presence of electrons, ions within an RPC. For this purpose, we have considered two approaches: representation of the space charge cloud as (a) a collection of ring charges, and (b) as a collection of line charges. The results from these different methods have been compared with the results available in the literature.

KEYWORDS: Resistive-plate chambers; Detector modelling and simulations II (electric fields, charge transport, multiplication and induction, pulse formation, electron emission, etc); Gaseous imaging and tracking detectors; Avalanche-induced secondary effects

¹Corresponding author.

Contents

1	Introduction	1
2	Calculation of positions of electron and ion cluster	2
3	Calculation of the electric field due to the space charge distribution	2
3.1	Ring approximation (method A)	2
3.1.1	Components of Electric field vector due to ring	2
3.2	Straight-line approximation with uniform charge density (method B)	3
3.2.1	Components of Electric field vector due to a charged line	4
3.3	Method available in literature (method C)	4
4	Results and discussions	5
4.1	Results of case-1	5
4.2	Results of case-2	5
5	Conclusions	7
A	Acknowledgement	7

1 Introduction

Resistive plate chamber (RPC)[1, 2] is a popular gaseous detector used to detect charged particles. It is basically made of two parallel resistive bakelite or glass plates. The space between the electrodes contained a particular gas mixture and a high-voltage (say $\pm 5kV$) is applied at each plate. When high energy charged particle pass through the RPC, it can knock out some primary electrons from gas molecules along its path. As an effect of the high electric field inside the gas gap of RPC, those primaries are accelerated towards the electrodes and produce secondaries by the ionization process. This process continues and develops an avalanche of numerous electrons and ions. An signal pulse is induced due to the movement of electrons in a pick-up strip placed on the detector [3]. So It is clear that to investigate the detector physics of RPC, we need to simulate that avalanche process very precisely. We know that space charge plays a crucial role while an avalanche is developing. So for simulation of an avalanche, the electric field due to space charge needs to be calculated dynamically.

In this paper, we intend to discuss three different methods (A, B, C) to calculate the electric field in the presence of the space charge. The method-A and C (see section 3.1 and 3.3) contains modeling of the space charge region as several co-centric charged rings of gradually increasing radius as in ref. [4]. Again, a ring can be thought of as a collection of charged straight lines (see section 3.2) of equal length S , which is our method-B. Now two cases need to be discussed:

Case-1: the linear charge density (λ) of a ring is kept constant in methods A and C. The lines corresponding to a ring have been shared the equal amount of charge (λS) to the method-B.

Case-2: the condition for the rings is remaining identical, as in case-1. However, the charges of lines have been calculated separately. We then compare the electric fields for these lines and rings in two cases. In this initial phase we are ignoring the reflections of charges on the ground plates. This is a serious matter and will be taken up in subsequent work.

2 Calculation of positions of electron and ion cluster

An avalanche has been simulated inside an RPC of dimension 30 cm \times 30 cm and a 2 mm gas gap, from an electron created at the origin (0,0,0) using the Garfield++ simulation tool [5]. The gas mixture containing 97% of $C_2H_2F_4$, 2.5% of $i - C_4H_{10}$ and 0.5% of SF_6 has been selected. A uniform electric field of 50kV/cm is applied perpendicularly to the parallel plates of the detector (which is considered here as z-direction) to perform this simulation. The operating pressure of the gas has been kept equal to one atmospheric pressure at temperature 293.15K. The Garfield++ can keep track of the drifting position and time of each primary and secondary electrons and ion generated during the avalanche. A table of position and corresponding time of those electrons and ions has been formed to calculate interpolated positions of electrons at a certain instant of time. The interpolated positions of space charge cloud at 18 ns, has been shown in figure 1a.

3 Calculation of the electric field due to the space charge distribution

3.1 Ring approximation (method A)

It is assumed that the avalanche charge distribution has a rotational symmetry about the z-axis as apparent from figure 1a. Along the z-direction, the gas gap g can be divided into N_z steps with the step size $\delta z = \frac{g}{N_z}$. The space charge region along the X-Y plane can also be divided into a number (N_r) of concentric charged rings centered at z-axis and of gradually increasing radius r (see figure 1b). The size of the ring $\delta r = \frac{r_{max}}{N_r}$ and δz have been chosen according to the transverse and longitudinal spread of the avalanche, e.g. $\delta r = \delta z = 0.001$ cm and $r_{max} = 0.045$ cm. Now, starting from a height $z = \bar{z}$ ($\bar{z} < g$), if any charge is present then the electric field due to all N_r rings has been calculated by doing numerical integration of the equation (3.1) and (3.3) and then the value of z set to $z + \delta z$. This process is iterated till $z_{max} = g$. In this method, the whole region of space charge can be covered to calculate the electric field. The calculated components of the field due to all rings are summed to get the total electric field at any point.

3.1.1 Components of Electric field vector due to ring

The X,Y and Z components of electric field at any position (x,y,z) due to a ring of radius r and of uniform charged density λ (see figure 1c), centered at z-axis can be written as follows,

$$\left. \begin{aligned} E_x^A &= \frac{\lambda r}{4\pi\epsilon_0} \int_0^{2\pi} \frac{(x-r \cos(\phi))}{\Delta} d\phi, & E_y^A &= \frac{\lambda r}{4\pi\epsilon_0} \int_0^{2\pi} \frac{(x-r \sin(\phi))}{\Delta} d\phi \\ E_z^A &= \frac{\lambda r}{4\pi\epsilon_0} \int_0^{2\pi} \frac{(z-\bar{z})}{\Delta} d\phi \end{aligned} \right\} \quad (3.1)$$

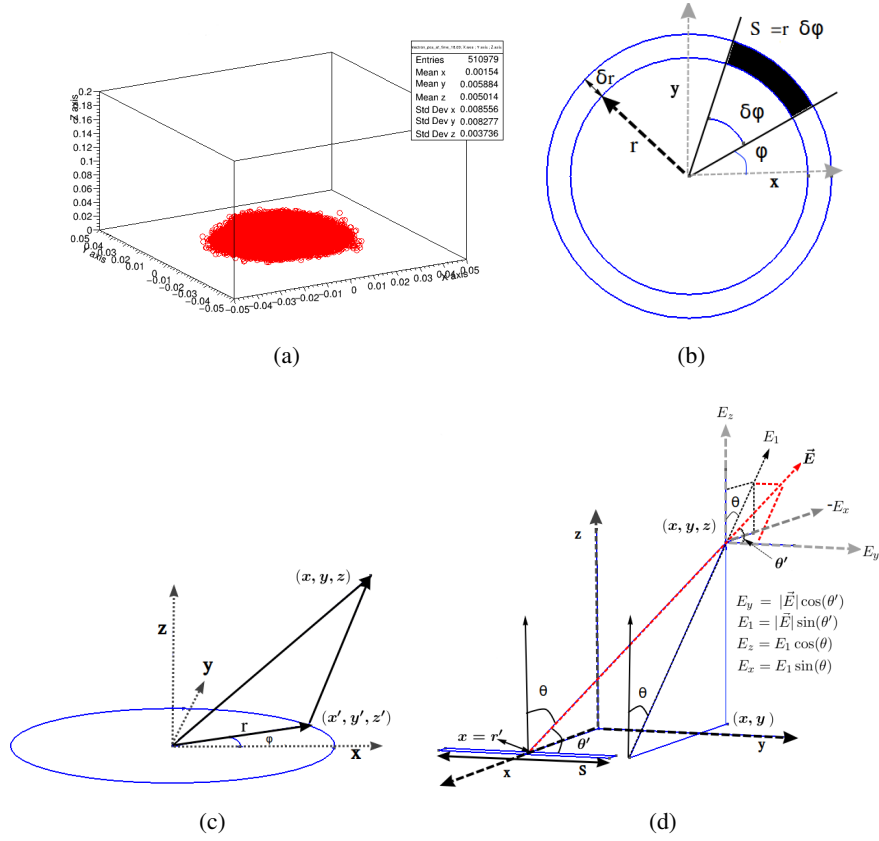


Figure 1: (a) The position of electron clouds at time 18 ns where the total number of electron is 510979. (b) picture of a ring of width δr (c) Computation of electric field due to charged ring. (d) Components of the electric field due to line charge.

where, $\Delta = [(x - r \cos(\phi))^2 + (y - r \sin(\phi))^2 + (z - \bar{z})^2]^{\frac{3}{2}}$, \bar{z} is the position of center of that ring along z -axis, and ϕ is the angular displacement of an element of ring of length $r\delta\phi$ from the x -axis (see figure 1b). If Q_{ring} is total charge of that ring then $\lambda = \frac{Q_{ring}}{2\pi r}$.

3.2 Straight-line approximation with uniform charge density (method B)

A ring can be equally segmented into a number of straight-lines. If r and δr are the radius and thickness of that ring respectively, then the length of an arc of any segmented element of that ring is $S=r \delta \phi$, where $\delta \phi$ is the angle in radian, subtended to the center of the circle (see figure 1b). S can be approximated as a straight-line of length S and thickness δr , when $\delta \phi$ is very small i.e. $S/r \leq 1$. It is discussed in section 3.1 that the space charge region can be divided into a number of rings. As an extension of this algorithm, those rings are also split into a number of straight lines, where $\delta \phi$ is chosen by the user. Therefore, the electric field can be calculated for each charged straight-line (for case-1 and case-2 in section 4) corresponding to a ring using the equations (3.2). Thus, after the formation of a ring by a number of straight lines the same iteration process discussed in section 3.1 can be followed to get electric fields for all charges. The components of fields of each charged line

are added iteratively to get the total electric field. Thus we can reproduce the results of the electric field of charged rings using the line charge approximation.

3.2.1 Components of Electric field vector due to a charged line

Let us consider a straight line of constant charged density $\bar{\lambda}$ and of length S , aligned parallel to the y-axis at $x = \bar{r}$, and $z = \bar{z}$. The X, Y, Z components of the electric field at any position (x,y,z) due to this straight line can be written as follows (see figure 1d),

$$\left. \begin{aligned} E_x^B &= \frac{\bar{\lambda}(x-\bar{r})}{4\pi\epsilon_0 P^2} \left[\frac{(y+\frac{S}{2})}{\sqrt{(y+\frac{S}{2})^2+P^2}} - \frac{(y-\frac{S}{2})}{\sqrt{(y-\frac{S}{2})^2+P^2}} \right], E_y^B = -\frac{\bar{\lambda}}{4\pi\epsilon_0} \left[\frac{1}{\sqrt{(y+\frac{S}{2})^2+P^2}} - \frac{1}{\sqrt{(y-\frac{S}{2})^2+P^2}} \right] \\ E_z^B &= \frac{\bar{\lambda}(z-\bar{z})}{4\pi\epsilon_0 P^2} \left[\frac{(y+\frac{S}{2})}{\sqrt{(y+\frac{S}{2})^2+P^2}} - \frac{(y-\frac{S}{2})}{\sqrt{(y-\frac{S}{2})^2+P^2}} \right] \end{aligned} \right\} \quad (3.2)$$

where, $P = \sqrt{(z-\bar{z})^2 + (x-\bar{r})^2}$, and if Q_{st} is the total charge of this straight line then, $\bar{\lambda} = \frac{Q_{st}}{S}$.

For a chosen value of $\delta\phi$ it can be said that the total number of straight-line needs to form a ring is $N_{st} = \frac{360}{\delta\phi}$. So $\delta\phi$ is the minimum angle that has to rotate to reach from one segment to another nearest segment. Necessary coordinate transformations have been carried out to evaluate electric field in a consistent frame of reference.

3.3 Method available in literature (method C)

The equation of the electric field at any point (ρ, α, z) in cylindrical co-ordinate system due to a ring of uniform charged density λ and radius "a" centered at z-axis, can also be found in ref. [6](v. I pp. 176), (see figure 1c),

$$\left. \begin{aligned} \vec{E}_{ring}^C(\rho, z, a) &= \frac{\lambda a}{\pi\epsilon_0} \left[\frac{1}{2\dot{r}_1\rho} \left(K_1(u) - \frac{(a^2 - \rho^2 + z^2)K_2(u)}{\dot{r}_1^2(1-u^2)} \right) \hat{\rho} + \frac{zK_2(u)}{\dot{r}_1^3(1-u^2)} \hat{z} \right] = E_r^C \hat{\rho} + E_z^C \hat{z} \\ u &= \frac{2\sqrt{a\rho}}{\dot{r}_1}, \dot{r}_1 = \sqrt{(a+\rho)^2 + z^2} \end{aligned} \right\} \quad (3.3)$$

where E_r^C, E_z^C are the radial and z- components of electric field and $K_1(u)$ and $K_2(u)$ are the complete elliptic integrals of first and second kinds.

The components of fields calculated in Cartesian co-ordinates (for method A and B) have been converted into cylindrical co-ordinates by using "Jacobi transformation" to compare with the results of method C. The required Jacobi matrix for this transformations is given below,

$$\begin{pmatrix} E_r^i \\ E_\alpha^i \\ E_z^i \end{pmatrix} = \begin{pmatrix} \cos(\alpha) & \sin(\alpha) & 0 \\ -\sin(\alpha) & \cos(\alpha) & 0 \\ 0 & 0 & 1 \end{pmatrix} \begin{pmatrix} E_x^i \\ E_y^i \\ E_z^i \end{pmatrix}, \quad \alpha = \tan^{-1}\left(\frac{y}{x}\right) \quad (3.4)$$

E_r^i, E_α^i, E_z^i are the radial, α and z directional components of electric fields at a position (ρ, α, z) of any charged ring or line. Where, $x = \rho \cos(\alpha)$, $y = \rho \sin(\alpha)$ and $z=z$ and $i = A, B$ for method-A and method-B respectively. These cylindrical form of the components for different methods can be represented together as $E_r^{A,B,C}, E_\alpha^{A,B}, E_z^{A,B,C}$.

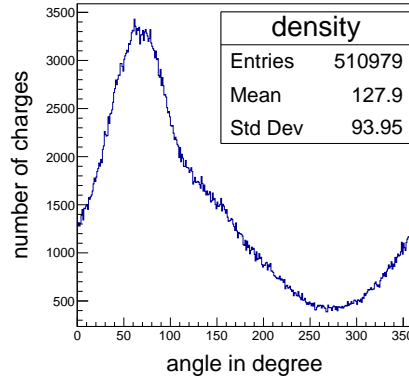


Figure 2: Angular distribution of charges at time 18 ns

4 Results and discussions

The integrations of equations (3.1) and (3.3) have been solved numerically by using standard "GSL-Integrator" from "GSL-library" available in "root 6.18/04" [7, 8]. The absolute values of calculated electric field components are set to zero when it goes below a minimum number $\epsilon = 10^{-8}$, because at this range the field due to the space charge is negligible in comparison to the applied field. The results can be divided into two cases:

case-1: The charge density λ has been considered constant in equations (3.1) and (3.3) of methods A,C. In method-B the charge (Q_{ring}) of a ring is equally shared between segmented lines from that ring, which is $Q_{st} = \lambda S = \frac{Q_{ring} S}{2\pi r}$ for a line.

case-2: In this case, the conditions for equations (3.1) and (3.3) remain the same as in the above **case-1**. However, in the actual scenario the angular distribution of the total Q_{ring} charge may not be uniform over the ring. Therefore, the amount of charge Q_{st} will be different for different N_{st} line of that ring. So charges are calculated separately for each line. Distribution of the charges reside on each line at different angles for all radius and height, have been shown in figure 2.

4.1 Results of case-1

It is well known to us that the electric field component E_z is dominating over E_r and E_α on the z-axis of a uniformly charged ring. Because of the axial symmetry, the components E_r and E_α cancel out each other and become zero. It can also be verified from the figures 3a, 3b and 3c, where the components of electric field $E_r^{A,B,C}$, $E_\alpha^{A,B}$, $E_z^{A,B,C}$ have been plotted for three different methods A,B,C. Again, from the same figure 3a it is clear that the ratios $E_z^C/E_z^A = E_z^C/E_z^B = 1$ on the z-axis. However, The values of $E_r^{A,B,C}$, $E_\alpha^{A,B}$ are always zero on the z-axis, so the calculation of their ratios is not possible. Hence, the ratio plot is not shown in the figures 3b and 3c.

4.2 Results of case-2

The magnitudes of E_z components for three methods A,B,C ($E_z^{A,B,C}$) are the same which can be verified from the figure 4a. But there are discrepancies between the radial and α components of

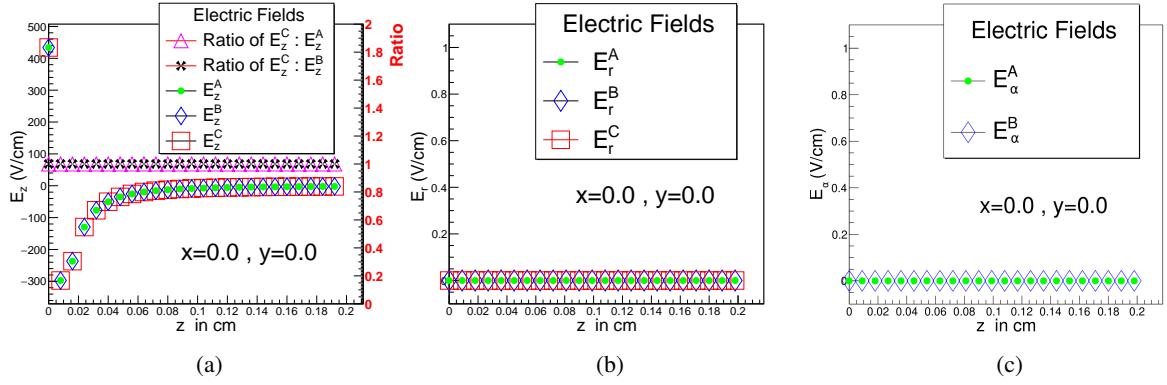


Figure 3: Computation of electric field components for case-1(section 4.1) on the z-axis. (a) The variation of $E_z^{A,B,C}$ on the z-axis has shown in the left-side axis of the figures and right side axis contain the corresponding ratios of the field components between E_z^C and $E_z^{A,B}$, (b) variation of $E_r^{A,B,C}$ on the z axis, (c) variation of $E_\alpha^{A,B}$ on the z axis.

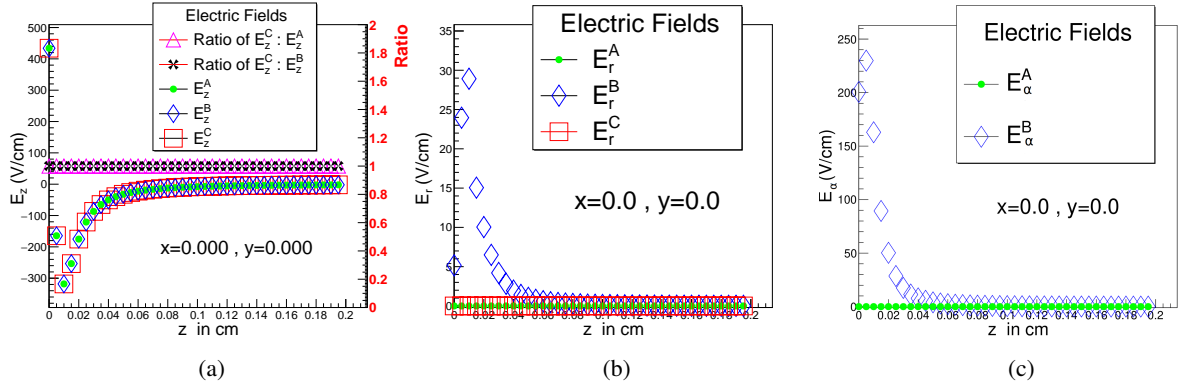


Figure 4: Computation of electric field components for case-2(section 4.2) on the z-axis. (a) The variation of $E_z^{A,B,C}$ on the z-axis has shown in the left-side axis of the figures and right side axis contain the corresponding ratios of the field components between E_z^C and $E_z^{A,B}$, (b) variation of $E_r^{A,B,C}$ on the z axis, (c) variation of $E_\alpha^{A,B}$ on the z axis.

electric field calculated in method-B (E_r^B, E_α^B) and method-A,C ($E_r^{A,C}, E_\alpha^{A,C}$) which is shown in the figures 4b and 4c. The components $E_r^{A,C}, E_\alpha^{A,C}$ still gives the same result zero along the z-axis as in case-1 for method-A and C. However, the components E_r^B, E_α^B is showing a non zero value. Especially near the charge distribution, the value is much higher than zero. These discrepancies can be explained from the angular distribution of charges shown in figure 2. It is clear from the same figure 2 that the nature of this angular distribution is not uniform; instead, it is observed that most of the charges are within the angular range from 0 to 150 degrees.

5 Conclusions

Initially, it was assumed that the nature of the electron cloud has some axial symmetry about the z -axis. So due to this symmetry, one can easily neglect the E_α component. Subsequently, from the analysis of an avalanche from a single primary electron it is observed that the angular charge distribution is not uniform, so the component E_α plays a significant role while avalanche is developing. Hence, it can't be ignored anymore. It is already discussed that the avalanche is generated here from a single primary electron. However, in an actual event, the avalanche can be formed from several primaries. So the results for that case along with the reflections of charges on the ground plates need to be found, which is also our future interest.

The merit of using straight line-approximation is that it produces similar results as uniformly charged rings as well as it can be easily used when the charged density is nonuniform over the ring. Again the most remarkable feature of the same is the components of field equations do not contain any elliptical integrals. So we do not need to worry about the numerical integrations.

A Acknowledgement

I am grateful to the members of INO collaboration and HEP experiment division of VECC for providing me the opportunity to do research. I would like to thank Prof. Nayana Majumdar for intense discussion and valuable suggestions.

References

- [1] R. Santonico and R. Cardarelli, *Development of resistive plate counters*, *Nuclear Instruments and Methods in Physics Research* **187** (1981) 377–380.
- [2] R. Cardarelli, R. Santonico, A. Biagio and A. Lucci, *Progress in resistive plate counters*, *Nuclear Instruments and Methods in Physics Research Section A: Accelerators, Spectrometers, Detectors and Associated Equipment* **263** (1988) 20 – 25.
- [3] F. Sauli, *Gaseous Radiation Detectors: Fundamentals and Applications*, vol. 36. Cambridge University Press, 8, 2014, [10.1017/CBO9781107337701](https://doi.org/10.1017/CBO9781107337701).
- [4] C. Lippmann and W. Riegler, *Space charge effects in resistive plate chambers*, *Nucl. Instrum. Meth. A* **517** (2004) 54–76.
- [5] H. Schindler, *Garfield++ user's guide*, <https://garfieldpp.web.cern.ch/garfieldpp> (April, 2020) .
- [6] E. Durand, *Électrostatique*. Masson et C^{ie}, 1964.
- [7] *Root data analysis framework user's guide*, <https://root.cern.ch/root/html/doc/guides/users-guide/ROOTUsersGuideA4.pdf> (May, 2018) .
- [8] R. Brun and F. Rademakers, *ROOT: An object oriented data analysis framework*, *Nucl. Instrum. Meth. A* **389** (1997) 81–86.